*Turkish Journal of Civil Engineering, 2025, xxxx-xxxx, Paper xxx,* ***Research Article***

# A Critical Evaluation of the Coefficient Method, Capacity Spectrum Method and Modal Pushover Analysis for Irregular Steel Buildings in Seismic Zones

**Vahid MOKARRAM**[1*]
**Mahmoud Reza BANAN**[2]
**Mohammad Reza BANAN**[3]
**Abdollah KHEYRI**[4]

## ABSTRACT

Classical design procedures are less advantageous than performance-based seismic design (PBSD) of buildings, which is included in existing standards such as ASCE 41-23 for new buildings or retrofitting. PBSD requires accurate assessment of building seismic responses. Such assessments can be done using either faster nonlinear static procedures (NSPs) or more time-intensive nonlinear time-history analyses (NTHAs). However, the reliability of NSPs can be questionable, as shown by previous research. Practitioners need to conduct further investigations to determine safety margins and the applicability scope of these methods. This is especially important for irregular buildings and near-fault zones. This problem is investigated in this paper by first using 1250 single-degree-of-freedom (SDOF) systems to evaluate the ASCE 41-23's coefficient method and performing 25000 NTHAs for near- and far-fault records. Second, the responses obtained from two alternative approaches, the modal pushover analysis (MPA) and FEMA 440's capacity spectrum method (CSM), are compared with NTHA responses for buildings with significant higher-mode effects. American standards are used to design 96 3D symmetric and asymmetric steel moment-resisting frame (MRF) buildings with different characteristics such as lateral, lateral-torsional, and torsional modes of vibration dominance as well as different stability conditions, which are considered in this paper. The MPA and CSM are compared with NTHAs in this paper. The results show

Note:
- This paper was received on January 21, 2024 and accepted for publication by the Editorial Board on July 25, 2024.
- Discussions on this paper will be accepted by xxxxxxx xx, xxxx.

• https://doi.org/10.18400/tjce.1422919

1 Jahrom University, Department of Mechanical Engineering, Jahrom, Fars, Iran
mokarram@jahromu.ac.ir - https://orcid.org/0000-0001-9820-6485

2 Shiraz University, Department of Civil and Environmental Engineering, Shiraz, Fars, Iran
bananm@shirazu.ac.ir - https://orcid.org/0000-0002-9763-8283

3 Shiraz University, Department of Civil and Environmental Engineering, Shiraz, Fars, Iran
banan@shirazu.ac.ir - https://orcid.org/0000-0002-7150-5343

4 Shiraz University, Department of Civil and Environmental Engineering, Shiraz, Fars, Iran
abdkheyri@gmail.com - https://orcid.org/0009-0004-9628-6986

* Corresponding author

that the ASCE 41-23's coefficient method is unreliable for near-fault zones and that the MPA and CSM are unreliable for seismic evaluation of buildings with dominant lateral-torsional modes of vibration or significant P-Δ effects. The results also revealed that MPA is a conservative approach for seismic evaluation of torsionally dominant buildings while CSM is not.

**Keywords:** Nonlinear static procedure, modal pushover analysis, capacity spectrum method, performance-based seismic design, irregular buildings, near-fault earthquakes.

## 1. INTRODUCTION

Regarding the high computational costs of performing NTHA, especially for design purposes where the analysis-design cycle has to be recursively repeated until the designer reaches the desired design, NTHAs are not widely used by designers in the everyday design of buildings. There have been notable attempts (see [1,2]) to bring the NTHA-based design of buildings to a computationally affordable level, but the computational costs of these problems are still a challenge, even with today's modern computers. The computational cost is not the only challenge for engineers, as the expertise required for modeling and designing buildings based on NTHAs also discourages the designers from undertaking such an approach. Thus, in present-day circumstances, NSPs are, in fact, a valuable substitute for NTHA, and are being prescribed by many guidelines including [3-5] to enable designers to adopt the PBSD approach for evaluation and retrofitting of existing buildings as well as designing new ones. The literature contains serious critiques of the accuracy of such approaches and more research is therefore required to determine the applicability scope of NSPs. A brief overview of the problem is therefore given here.

The project initiated by the Federal Emergency Management Agency (FEMA) in 1984 to address the seismic risk of existing buildings marked the beginning of PBSD in building codes and standards. The project resulted in the FEMA 273 [6] report, which established quantitative acceptance criteria for four performance levels: Operational (OP), Immediate Occupancy (IO), Life Safety (LS), and Collapse Prevention (CP). FEMA 273 [6] introduced the fundamental concepts that were adopted by subsequent guidelines such as FEMA 356 [3] and FEMA 440 [4]. The NSP coefficients proposed in FEMA 356 [3] have been continuously revised and enhanced in later guidelines such as FEMA 440 [4]. This method also forms the basis of the codified coefficient method in recent seismic building standards such as ASCE/SEI 41-23 [5]. There are also many other NSPs, including adaptive and multi-mode approaches, available in the literature other than the aforementioned codified procedures. Some of them comprise the N2 method [7,8], the MPA [9,10], the upper-bound pushover analysis (UBPA) [11], the adaptive modal combination (AMC) procedure [12], the adaptive capacity spectrum method (ACSM) [13], the consecutive modal pushover (CMP) [14], the generalized pushover analysis (GPA) procedure [15], and the normalized multi-mode nonlinear static (NMP) procedure [16].

Kalkan and Kunnath [17] evaluated four NSPs, namely MPA, UBPA, AMC, and FEMA 356 NSP methods, for seismic evaluation of buildings using NTHAs with different ground motions, and found that the AMC procedure was the most consistent and accurate. Similarly, Bento et al. [18] assessed four NSPs, namely FEMA 440's CSM, N2, MPA, and ACSM procedures, for seismic assessment of plan-irregular reinforced concrete (RC) buildings using

a full-scale experimental frame and NTHAs, and found that the ACSM performed better than the others in predicting both global and local responses. By considering sixteen 2D frames, Pinho et al. [19] compared five NSPs, namely CSM, N2, MPA, AMC, and ACSM procedures, for seismic assessment of building frames with nonlinear dynamic analysis results, and found that MPA and ACSM performed slightly better than the others. However, Fragiadakis et al. [20] demonstrated that the accuracy of NSPs depends on the building characteristics, the level of inelastic demand and engineering demand parameters. Allahvirdizadeh and Gholipour [21] argued that pushover methods have considerable flaws in identifying critical plastic regions. This problem becomes more severe at higher performance levels (i.e., higher nonlinearities). Moreover, Gonzalez-Drigo et al. [22] showed that using NSPs in damage state studies can lead to unconservative estimates. Marino et al. [23] investigated the near-collapse in-plane global response of unreinforced masonry buildings and showed that the European and Italian NSPs did not yield conservative results. Ruggieri and Uva [24] assessed the new NSP in the Italian building code by examining some low-rise RC buildings and inferred that it might produce more accurate results, but it also might yield non-conservative results in contrast to the conventional NSP, and therefore, it requires further validation with NTHA. Daei and Poursha [25] evaluated various NSPs, such as MPA, force-based adaptive pushover, displacement-based adaptive pushover, etc., for estimating the seismic demands of RC buildings and compared them with NTHA. They demonstrated that the accuracy of NSPs varies with the structure's height and the ground motion type. They also revealed that none of the NSPs had a significant advantage over the others and recommended further research and improvements of NSPs.

Some researchers have tried to adopt NSPs for approximating the structural capacity instead of using sophisticated incremental dynamic analysis (IDA). Ferraioli [26] investigated the dynamic increase factor (DIF) for NSP of RC frame buildings against progressive collapse due to sudden column loss. It was found that the DIF depended on the building properties, the location of the removed column, the catenary action of the floor slab, and the plastic dissipation capacity. Ke et al. [27] developed a multi-stage-based NSP based on the energy balance concept and a trilinear kinematic model to estimate the seismic demands of steel MRFs equipped with steel slit walls and compared its performance with NTHA responses. They concluded that the multi-stage-based NSP was able to produce satisfactory and conservative estimates of the peak seismic demands of the considered steel MRFs and that the seismic demand was significantly influenced by the multi-yielding stages of the system. Couto et al. [28] assessed old RC buildings in Lisbon using the N2 method and investigated how aging, smooth rebar, and corrosion affected seismic capacity and fragility. Wang et al. [29] proposed a deformation-based pushover analysis (DPA) method for evaluating the transverse seismic performance of tall inverted Y-shaped pylons in kilometer-span cable-stayed bridges. They applied the DPA to a case study of Sutong Bridge and compared it with other methods such as IDA, conventional NSP, and MPA. They concluded that DPA was efficient and convenient for the preliminary seismic design of inverted Y-shaped bridge pylons.

In addition to the individual application of NSPs and NTHAs, some studies have used them in combination to reduce the computational costs of the problem. For instance, Mokarram and Banan [2] proposed an effective adaptive surrogate multi-objective optimization model called surrogate FC-MOPSO in which optimal automated PBSD of buildings could be performed by simultaneous utilization of NSP and NTHAs such that the final designs were

based on NTHAs. They showed that up to 92% reduction in the required NTHAs could be achieved using their proposed model. Rossetto et al. [30] compared different methods for analyzing building responses under sequential earthquake and tsunami demands. They used a 10-storey RC structure as a case study. They found that a dynamic earthquake analysis followed by a variable depth pushover tsunami analysis was the best alternative to full dynamic analyses.

The frequency spectrum of seismic ground motions, which varies significantly between near-field and far-field events, influences the structural response of buildings. For instance, Bhandari et al. [31] assessed the seismic risk of a base-isolated building under near- and far-field earthquakes and found that the PGV:PGA ratio of near-field earthquakes affected the damage probability. Mokarram et al. [32] demonstrated that the maximum displacement ratio in ASCE/SEI 41-17's coefficient method can yield unconservative results for near-fault sites. Bilgin and Hysenlliu [33] have also shown that response of the masonry buildings under near-field and far-field earthquakes is remarkably different. Caution must be exercised when using NSPs in near-fault zones since they can yield unconservative solutions (see [34,35]).

About the criticisms pointed out in this section, it becomes evident that the NSPs, although widely used by practitioners for performing PBSDs, still have questionable reliability. Furthermore, a significant amount of research on the NSPs has been dedicated to evaluating the seismic vulnerability of regular buildings. Therefore, as confirmed by the review article by Asıkoğlu et al. [36], it is essential to examine their reliability regarding the impact of building irregularity on seismic behavior. This problem is even more magnified by noting that many failures have occurred due to asymmetry and irregularity in structures, during past earthquakes Das et al. [37]. Near-fault earthquakes also pose another concern as stated earlier. Thus, in this paper, ASCE/SEI 41-23's [5] coefficient method is evaluated first as the most practical code-based single-mode NSP for near- and far-fault earthquakes. Secondly, the accuracy of two alternative NSPs, namely FEMA 440's [4] CSM and MPA [9,10], for seismic assessments of symmetric and irregular steel MRF buildings with various characteristics is evaluated. As Najam [38] asserts, MPA method is the most well-known multi-mode NSP in the literature that incorporates the effects of higher modes contributions in system's response. Hassan and Reyes [39] also deduced that MPA is a strong candidate for approximating the inelastic seismic demands for the RC MRFs without dampers, instead of using the more complex NTHA.

## 2. NONLINEAR SYSTEMS MODELING

The modified Ibarra-Krawinkler (IK) hysteresis model, proposed by Lignos and Krawinkler [40], in conjunction with the concentrated plastic hinge (CPH) model developed by Zareian and Medina [41], is utilized within the OpenSees [42] library for numerical simulation purposes of SDOF systems. The modified IK model [40], which is based on moment-rotation curves, aligns very well with FEMA documents and ASCE/SEI 41-23 [5] procedures for nonlinear analysis. This makes it highly adaptable for performing NTHA and NSP with a range of structural materials [40,43,44]. It effectively captures the response to cyclic loading, including strength and stiffness degradation in steel structures [40].

Rayleigh damping is commonly employed in dynamic analysis and is expressed by Eq. (1).

$$\mathbf{C} = a_0\mathbf{K} + a_1\mathbf{M} \quad (1)$$

where **K** and **M** denote initial stiffness and mass of the structure, respectively. $a_0$ and $a_1$ are stiffness-proportional and mass-proportional constants, respectively. However, initial stiffness-based Rayleigh damping can result in overestimated damping forces during NTHAs. More precise predictions of inelastic response can be obtained using tangent stiffness proportional damping [45,46], although this approach necessitates continuous updating of damping coefficients in the nonlinear problem. The CPH model, as proposed by Zareian and Medina [41], involves attaching nonlinear springs to the ends of the original six degrees of freedom (DOF) beam element. This creates an equivalent elastic beam element with end nonlinear rotational springs, resulting in eight DOFs. By assigning the stiffness-proportional damping coefficient to the linear beam element (Fig. 1), the model prevents excessively large damping forces that can occur due to system softening in the nonlinear phase. Zareian and Medina [41] demonstrated that this method yields results consistent with those obtained using tangent stiffness methods. When combined with the modified IK material model, the CPH model [41] suggests effectiveness for PBSD of steel MRFs [47]. In case ASCE/SEI 41-23 [5] moment-rotational behaviors are adopted for nonlinear springs, the P-M interactional effects in 2D models can be accounted for since the moment-rotational behaviors are a function of the axial force in the element.

In this study, a 5% damping ratio is applied to define the design spectrum. However, for the execution of NTHA in compliance with ASCE/SEI 41-23 [5], a 3% damping ratio is utilized to establish the Rayleigh damping coefficients.

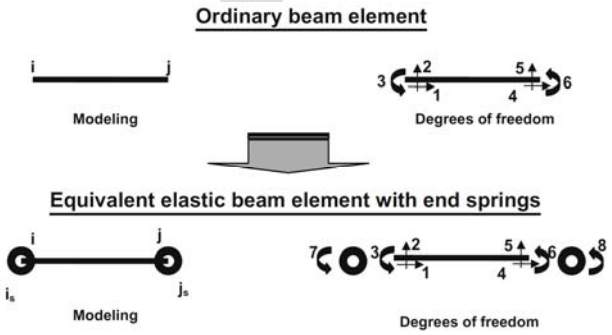


*Fig. 1 - Representation of the ordinary nonlinear beam element and its equivalent model comprised of an elastic beam element with nonlinear springs at both ends [41].*

## 3. EVALUATION OF ASCE/SEI 41-23'S [5] COEFFICIENT METHOD THROUGH SDOF SYSTEMS

The ASCE/SEI 41-23's [5] coefficient method is a single-mode NSP, which, as per ASCE/SEI 41-23 [5], is permitted to be used under two conditions: (1) the ratio of the elastic strength demand to yield strength (i.e., $\mu_{\text{strength}}$) must be smaller than the maximum strength ratio (i.e., $\mu_{\max}$) of the system, and (2) the effects of higher modes must not be significant.

In this section, an investigation will be conducted to determine whether the method is reliable for near-fault sites. The reliability of ASCE/SEI 41-23's [5] coefficient method will be examined by considering 1250 SDOF systems. The coefficient method responses of the SDOF systems are then evaluated using ten near-fault and ten far-fault earthquake records which entails performing 25000 NTHAs.

ASCE/SEI 41-23's [5] coefficient method imposes lateral loads on the multi-degrees-of-freedom (MDOF) system that follow the vertical distribution of the fundamental mode shape of the structure in the direction of analysis. Then, a pushover analysis is performed to determine the force-displacement curve of the structure (i.e., base shear versus control node displacement). The force-displacement curve is used to generate an idealized force-displacement curve according to the procedure in ASCE/SEI 41-23 [5]. Finally, the target displacement, $\delta_t$, of the control node, which represents the system displacement demand for a given hazard level, is computed from Eqs. (2) to (7).

$$\delta_t = C_0 C_1 C_2 S_a \frac{T_e^2}{4\pi^2} g \tag{2}$$

$$C_0 = \phi_{1,r} \frac{\sum_1^N m_i \phi_{i,n}}{\sum_1^N m_i \phi_{i,n}^2} \tag{3}$$

$$C_1 = 1 + \frac{\mu_{\text{strength}}}{a T_e^2} \tag{4}$$

$$C_2 = 1 + \frac{1}{800}\left(\frac{\mu_{\text{strength}}-1}{T_e}\right)^2 \tag{5}$$

$$\mu_{\text{strength}} = \frac{S_a}{V_y/W} C_m \tag{6}$$

$$T_e = T_i \sqrt{K_i/K_e} \tag{7}$$

Here, $C_0$ is a modification factor that relates the spectral displacement of an equivalent SDOF system to the roof displacement of the building MDOF system and is equal to unity for an SDOF system. $C_1$ is the maximum displacement ratio coefficient, which is a modification factor that relates the expected maximum inelastic displacements to the displacements computed for linear elastic response. $C_2$ accounts for the effect of pinched hysteresis shape, cyclic stiffness degradation, and strength deterioration on the maximum displacement response. $m_i$, $\phi_{1,r}$, $\phi_{i,n}$ denote the mass at level *i*, the ordinate of the first mode shape at the roof (control node), and the ordinate of mode shape *i* at level *n* of the building, respectively. $W$, $a$, $g$, $T_e$, and $C_m$ respectively represent, the effective seismic weight, the site class factor, the gravitational acceleration, the effective fundamental period of the building in the direction of interest, and the effective mass factor which is equal to unity for an SDOF system. $T_i$, $K_i$ and $K_e$ are the elastic fundamental period, elastic lateral stiffness, and effective lateral stiffness of the system, respectively. $S_a$ is the spectral acceleration at the effective fundamental period and damping ratio of the building in the direction of interest.

According to Eq. (1), ASCE/SEI 41-23's [5] coefficient method depends on the design response spectrum of the chosen site. In this section, a site located in Northridge, California

(34°14'17.9"N, 118°31'59.8"W) with Class D soil is considered. The 5% damped design spectrum for this site, as specified in ASCE/SEI 41-23 [5], is employed for the BSE-2N hazard level in this study. Earthquake records for each SDOF system were scaled to align with the design spectrum, in accordance with ASCE 7-22's [48] amplitude scaling method. A period range from $0.2T_i$ to $1.5T_i$ was selected for this scaling process. Coefficient method evaluations are also derived from the same design spectrum. Newmark average acceleration method is adopted for conducting nonlinear time-history analyses. In addition, a Rayleigh damping ratio of 3% was applied for nonlinear time-history analyses, as per the ASCE/SEI 41-23 [5] provisions for NTHA.

To evaluate the reliability of the coefficient method, SDOF systems with various fundamental periods and force-displacement behaviors are considered. The mass of each SDOF system was adjusted to achieve a fundamental period of 0.1, 0.2, …, or 2.5 sec. Additionally, 50 different values of effective yield strength, $V_y$, ranging from 155 kN to 4700 kN were used for the SDOF systems. Therefore, a total of 1250 SDOF systems were obtained. For each of these SDOF systems, a nonlinear material behavior should also be defined. Hence, a recursive analysis was performed to adjust the yield stress of the material such that the evenly distributed values of effective yield strengths could be obtained. Moreover, the recursive analysis included identifying matching W-sections. Specifically, a W-section was assigned to each yield stress such that if the W-section were used in a 3.66 m (12 ft) high cantilever column with a concentrated mass at its top, and the column were analyzed using the ASCE/SEI 41-23 [5] coefficient method, the system would yield the required fundamental period and effective yield strength corresponding to one of the 1250 SDOF systems. Once the W-section with its specific yield stress is identified, the nonlinear material behavior of the SDOF system, based on ASCE/SEI 41-23 [5], is also established. This is because, in the recursive analysis, the moment-rotation behavior of the W-sections is derived from ASCE/SEI 41-23 [5] and assigned to the nonlinear spring at the base of the column, as described in Section 2. For instance, it was found that if a W 12×120 section is assigned to an SDOF column with a concentrated 141.15 kg mass at the top and an elastic element, and the backbone curve of this section with $F_y = 186.16$ MPa is assigned to the nonlinear spring at the base, performing the ASCE/SEI 41-23 [5] coefficient method would result in $V_y = 154.93$ kN and $T_i = 0.101$ sec, which matches one of the considered SDOF systems (i.e., with $V_y = 154$ kN and $T_i = 0.1$ sec). Therefore, the backbone curves obtained from the ASCE/SEI 41-23 [5] tables for a W 12×120 section with $F_y = 186.16$ MPa in steel moment-resisting frames are used for this specific SDOF system.

The nonlinear time-history response of each system was evaluated according to the ASCE/SEI 41-23's [5] nonlinear dynamic procedure (NDP) under ten far-fault (Table 1) and ten near-fault (Table 2) ground motion records. Near-fault and far-fault records adopted in this study are those that have distances to the fault rupture (i.e., $R_{rup}$ in Tables 1 and 2) that are less than and greater than ten kilometers, respectively. All records were recommended by FEMA 440 [4] for Class D soils. The average system responses under near-fault or far-fault ground motion records were used to assess the performance of the SDOF systems. Furthermore, for each fundamental period, the system responses were averaged over the responses of fifty SDOF systems with different shear yield strengths but the same fundamental period.

*Table 1 - Far-fault ground motion records employed in this paper for evaluation of ASCE/SEI 41-23's [5] coefficient method using SDOFs.*

| Event Name | Year | Station | RSN[(1)] | Mechanism | Magnitude | $R_{jb}$[(2)] (*km*) | $R_{rup}$[(3)] (*km*) | $V_s$[(4)] (*m/s*) |
|---|---|---|---|---|---|---|---|---|
| **San Fernando** | 1971 | Cholame-Shandon Array #2 | RSN60_SFERN_C02DWN | Reverse | 6.6 | 217.5 | 218.1 | 184.8 |
| **San Fernando** | 1971 | LA-Hollywood Stor FF | RSN68_SFERN_PEL090 | Reverse | 6.6 | 22.8 | 22.8 | 316.4 |
| **Morgan Hill** | 1984 | Gilroy Array #2 | RSN456_MORGAN_G02000 | Strike Slip | 6.2 | 13.7 | 13.7 | 270.8 |
| **Whittier Narrows-01** | 1987 | Downey-Birchdale | RSN614_WHITTIER_A_A-BIR090 | Reverse Oblique | 6.0 | 14.9 | 20.8 | 245.1 |
| **Whittier Narrows-01** | 1987 | LA-116th St School | RSN626_WHITTIER_A_A-116270 | Reverse Oblique | 6.0 | 18.2 | 23.3 | 301.0 |
| **Loma Prieta** | 1989 | Gilroy-Historic Bldg. | RSN764_LOMAP_GOF160 | Reverse Oblique | 6.9 | 10.3 | 11.0 | 308.6 |
| **Landers** | 1992 | North Palm Springs | RSN882_LANDERS_FHS000 | Strike Slip | 7.3 | 26.8 | 26.8 | 344.7 |
| **Landers** | 1992 | Yermo Fire Station | RSN900_LANDERS_YER270 | Strike Slip | 7.3 | 23.6 | 23.6 | 353.6 |
| **Northridge-01** | 1994 | Garden Grove-Santa Rita | RSN973_NORTHR_GAR000 | Reverse | 6.7 | 63.7 | 66.6 | 301.1 |
| **Northridge-01** | 1994 | Los Angeles-7-story Univ Hospital (FF) | RSN1007_NORTHR_UNI005 | Reverse | 6.7 | 32.4 | 34.2 | 322.3 |

(1)Record Sequence Number, which is a unique identifier for each ground motion record in the PEER ground motion database.

(2)The Joyner-Boore distance.

(3)Closest distance to the fault rupture.

(4)Average shear wave velocity over the top 30 meters of the subsurface.

*Table 2 - Near-fault ground motion records employed in this paper for evaluation of ASCE/SEI 41-23's [5] coefficient method using SDOFs.*

| Event Name | Year | Station | RSN[(1)] | Mechanism | Magnitude | $R_{jb}$[(2)] (*km*) | $R_{rup}$[(3)] (*km*) | $V_s$[(4)] (*m/s*) |
|---|---|---|---|---|---|---|---|---|
| **Loma Prieta** | 1989 | Los Gatos-Lexington Dam | RSN3548_LOMAP_LEX000 | Reverse Oblique | 7.0 | 3.2 | 5.0 | 1070.3 |
| **Kobe** | 1995 | Takatori | RSN1120_KOBE_TAK000 | Strike Slip | 6.9 | 1.5 | 1.5 | 256.0 |
| **Kobe** | 1995 | Kobe University | RSN1108_KOBE_KBU090 | Strike Slip | 6.9 | 0.9 | 0.9 | 1043.0 |
| **Kobe** | 1995 | Port Island (0 m) | RSN1114_KOBE_PRI000 | Strike Slip | 6.9 | 3.31 | 3.31 | 198.0 |
| **Erzican** | 1992 | Erzican | RSN821_ERZINCAN_ERZ-EW | Strike Slip | 6.7 | 0.0 | 4.38 | 352.1 |
| **Northridge-01** | 1994 | Rinaldi Receiving Sta | | Reverse | 6.7 | 0.0 | 6.5 | 282.3 |
| **Northridge-01** | 1994 | LA-Sepulveda VA Hospital | RSN1004_NORTHR_SPV270 | Reverse | 6.7 | 0.0 | 8.44 | 380.1 |
| **Northridge-01** | 1994 | Newhall-Fire Sta | RSN1044_NORTHR_NWH090 | Reverse | 6.7 | 3.16 | 5.92 | 269.1 |
| **Imperial Valley-06** | 1979 | El Centro-Meloland Geot. Array | RSN171_IMPVALL_H_H_EMO000 | Strike Slip | 6.5 | 0.07 | 0.07 | 264.6 |
| **Duzce** | 1999 | Duzce | RSN1599_DUZCE_ATS030 | Strike Slip | 7.1 | 0.0 | 6.6 | 281.9 |

[(1)]Record Sequence Number, which is a unique identifier for each ground motion record in the PEER ground motion database.

[(2)]The Joyner-Boore distance.

[(3)]Closest distance to the fault rupture.

[(4)]Average shear wave velocity over the top 30 meters of the subsurface.

Figs. 2(a) and (b) show the base shear demands obtained from the 1250 considered SDOF systems for far-fault and near-fault records, respectively.

Fig. 3 compares the relative errors of coefficient method estimations with NTHA responses. It reveals that the base shear demands from the coefficient method can be unreliable for near-fault sites, with errors up to 30%. For far-fault regions and structures with small fundamental periods (i.e., low-rise structures), the coefficient method provides conservative estimations of base shear demand of the system with errors that can reach 15%. Fig. 3 also suggests that the coefficient method can be a non-conservative method for medium to high-rise buildings in far-fault regions.

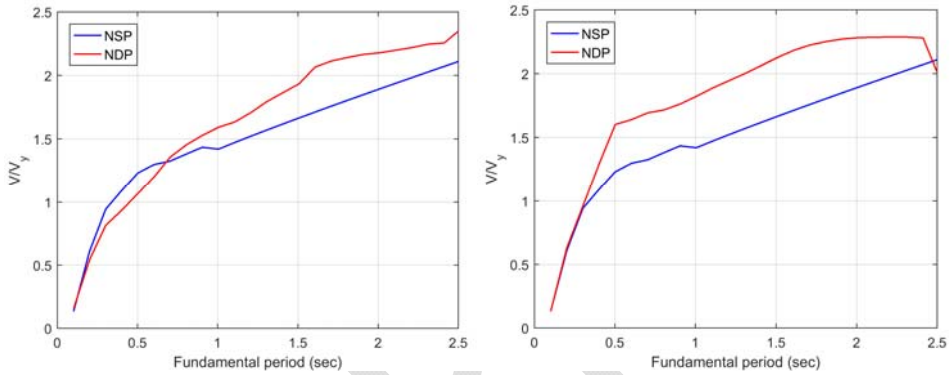


*(a)* *(b)*

*Fig. 2 - Normalized base shear demands from ASCE/SEI 41-23's [5] NSP (i.e., the coefficient method) and NDP for (a) far-fault, and (b) near-fault sites.*

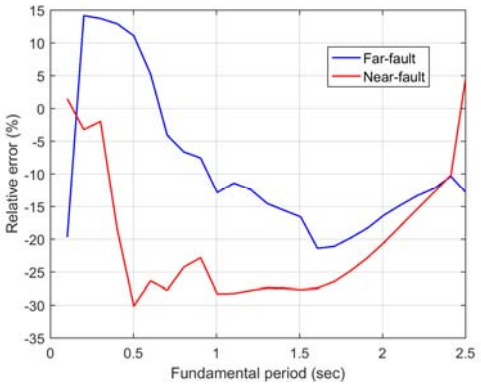


*Fig. 3 - Relative error of ASCE/SEI 41-23's [5] coefficient method with respect to the NDP in predicting base shear demands for far-fault and near-fault sites*

## 4. EVALUATION OF CSM AND MPA PROCEDURES FOR IRREGULAR BUILDINGS

In this section, it is examined whether FEMA 440's [4] CSM and MPA [9,10] procedures can be safely applied for seismic design and evaluation of irregular buildings. 96 3D buildings, of which 12 are symmetrical and the remaining 84 are unsymmetrical will be considered. The 84 unsymmetrical models are generated by modifying the first 12 symmetrical buildings to create 36 buildings with plan asymmetry and 48 buildings with different stability statuses.

### 4.1. Procedure

The 12 symmetrical buildings consist of 6 five-story and 6 ten-story buildings with either 5 m (Fig. 4(a)) or 10 m (Fig. 4(b)) bay spans. The buildings were designed to meet the requirements of ANSI/AISC 360-22 [49] and following the equivalent lateral force method and the load combinations of ASCE/SEI 7-22 [48] in three different categories: (1) ordinary steel MRFs, (2) special MRFs, and (3) designed for gravity loads only. The list of these 12 basic models is given in Table 3. It is noted the response modification factor (*R*-factor) for ordinary and special steel MRFs are equal to 3.5, and 8 as per ASCE/SEI 7-22 [48], respectively. Story heights in all models are equal to 3.6 m.

The dead load of the floors was taken equal to 4.1 kN/m$^2$ and an additional evenly distributed dead load of 1.5 kN/m$^2$ was applied to the floors to account for the loads of building partitions. The live load on building floors and the roofs were respectively taken equal to 2 kN/m$^2$ and 1.5 kN/m$^2$. The density, modulus of elasticity, yield, and ultimate strength of steel material were assumed to be 7850 kg/m$^3$, 200 GPa, 240 MPa, and 360 MPa, respectively. The configurations for the 12 basic building designs are given in Table A1 and Figs. A1, A2, A3, A4 and A5 of Appendix 1.

Force-based fiber elements in OpenSees [42], utilizing the Gauss-Lobatto integration method with five integration points, are employed in this section. For detailed discussions on the preference for force-based elements over displacement-based elements, refer to [50,51]. The Steel02 material in OpenSees [42] is used to model the uniaxial elasto-plastic behavior of the fibers. To ensure a more robust numerical analysis, a small strain hardening value of 1% was also incorporated. The 40-fiber discretization scheme, as discussed by Kostic and Filippou [52], was adopted. Kostic and Filippou [52] noted that even a 24-fiber scheme would achieve remarkable accuracy for I-shaped steel sections. In fiber element-based evaluation of the buildings the effects of rigid end zones are not accounted for.

The 36 buildings with asymmetrical plans were created by changing the mass distribution of 12 symmetrical buildings in three different ways. A part of the floor on the north-west panel was removed, and subsequently added some additional masses to points B2, B3, C2, and C3 of the plans of the basic buildings given in Fig. 4. This resulted in 36 buildings with three types of plan asymmetry, as explained below. Type 1 buildings have 9 times the removed mass added to each point B2, B3, C2 and C3. Type 2 buildings have 1.5 times the removed mass added to each point A1, A4, D1 and D4 and 2 times the removed mass added to each point where frames A, B, C, D intersect with frames 1 and 2. Type 3 buildings have 9 times the removed mass added to each point A1, A4, D1 and D4. The extra masses on the frames

were also adjusted so that the center of mass and the center of rigidity are 15% of the plan's dimension apart. Fig. 5 serves as an example, depicting the modification of model M1's plan. This alteration involves excising the shaded region from the plan and augmenting the mass at each of the four designated locations by a factor of nine, as shown in Fig. 5. To shift the building's center of mass by 2.7 meters-equivalent to 15% of the plan's dimensions-away from its center of rigidity, the masses placed on the frames along axes 2 and 3 are adjusted

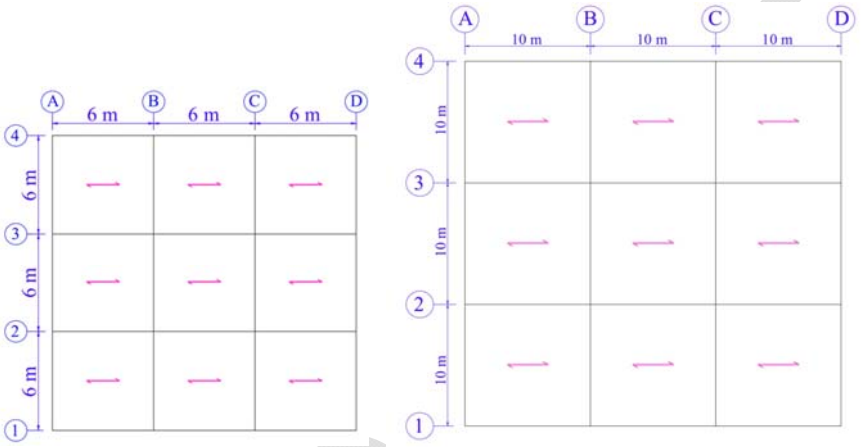


*(a)* *(b)*

*Fig. 4 - The two basic plans used for generating 96 symmetric and asymmetric five- and ten-story buildings with (a) 6 m bay spans, and (b) 10 m bay spans.*

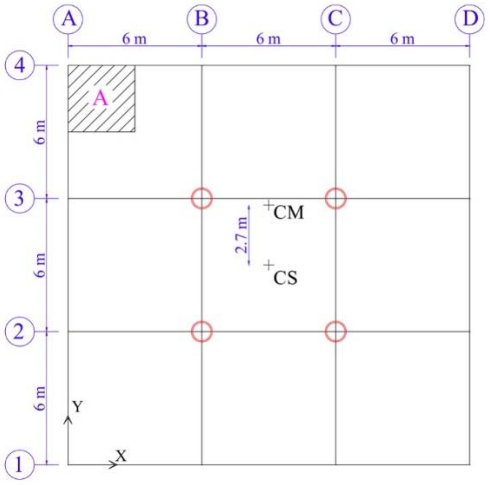


*Fig. 5 - Model M1's plan modified to generate its corresponding Type 1 asymmetric building (i.e., model M13).*

by factors of 0.1 and 1.9, respectively. Figs. 6 (a), (b), and (c) show the vibrational modes of three 5-story buildings with plan asymmetry, which were obtained by modifying model M1 of Table 3. The number of modes in these figures corresponds to the number of modes that achieved 90% mass participation. As an example, Table 4 lists the periods and effective mass participation factors for the initial modes of vibration in Type 1, Type 2, and Type 3 buildings (models M13, M25, and M36, respectively). It is ensured that the modes included in Table 4 provide at least 90% mass participation

Ultimately, buildings exhibiting different stability conditions were derived from eight of the basic symmetric buildings listed in Table 3 (i.e., models M1, M2, M4, M5, M7, M8, M10, and M11). To achieve this, the moments of inertia of the columns were changed in the north-south direction so that stability coefficients of 0.1 and 0.2 could be obtained. This was done for the first story, middle story, and top story of the 12 buildings. As a result, a suite of 8×2×3=48 buildings with different stability coefficients, as listed in Table 5, were generated. The sections of the columns that were modified due to stability conditions are detailed in Table A2 within Appendix 1. The stability coefficient is obtained from Eq. (8) as per ASCE/SEI 7-22 [48].

$$\theta = \frac{P_x/h_{sx}}{V_x/\Delta_{xe}} \tag{8}$$

where $P_x$ is the total vertical design load at and above level $x$, $V_x/\Delta_{xe}$ is the story stiffness at level $x$ calculated as the ratio of the seismic design shear, $V_x$, divided by the corresponding elastic story drift, $\Delta_{xe}$, and $h_{sx}$ is the story height below level $x$. The selected value of $\theta = 0.1$ in this study is critical because the ASCE/SEI 7-22 [48] standard states that P-Δ effects on story shears and moments, the resulting member forces and moments, and the story drift induced by these effects can be ignored when the stability coefficient is equal to or less than 0.10. Furthermore, according to the ASCE/SEI 7-22 [48] standard, if $\theta > \theta_{max}$, the building is potentially unstable and must be redesigned. Since $\theta_{max}$ cannot exceed 0.25, $\theta = 0.2$ was chosen to represent buildings with high stability problems. The stability coefficient in Eq. (8), which represents the impact of gravitational forces on stability, is linked to the building's story stiffness, represented by the story stiffness ratio $V_x/\Delta_{xe}$. By adjusting the columns' moments of inertia, this coefficient can be manipulated to highlight stability concerns at various building levels. Although this coefficient can be calculated for each story, this study demonstrates stability issues at the lower, middle, and upper stories of the building. Evidently, the stability issues included in the buildings of this section are explicitly accounted for in NTHA evaluations. Thus, NTHA analyses can be considered the reference method to which FEMA 440's [4] CSM, MPA [9,10] methods can be compared.

Based on the discussions in Section 2, the 96 buildings described in this section were modeled using OpenSees [42]. Then, the seismic responses of the buildings were evaluated using FEMA 440's [4] CSM, MPA [9,10], and the rigorous NTHA method. The NTHA was performed for the buildings using 14 horizontal records, scaled to the considered design spectrum, from the first seven earthquakes in Table 1. It is noted that each earthquake in Table 1 represents two horizontal records for a 3D building. A brief description of FEMA 440's [4] CSM and MPA [9,10] procedures is given below.

*Table 3 - List of the first 12 basic symmetric models.*

| Model No. | *R*-factor | Bays span (m) | Number of stories |
|---|---|---|---|
| **M1** | 3.5 | 6 | 5 |
| **M2** | 8.0 | | |
| **M3** | N/A* | | |
| **M4** | 3.5 | 10 | |
| **M5** | 8.0 | | |
| **M6** | N/A* | | |
| **M7** | 3.5 | 6 | 10 |
| **M8** | 8.0 | | |
| **M9** | N/A* | | |
| **M10** | 3.5 | 10 | |
| **M11** | 8.0 | | |
| **M12** | N/A* | | |

*Not applicable because the model was designed for gravitational loads only.

*Table 4 - Period and effective mass participation factors of three 5-story buildings with plan asymmetries of (a) Type 1 (model M13), (b) Type 2 (model M25), and (c) Type 3 (model M37).*

| Model | The mode of vibration | Period (sec) | Mass participation factor (%) | |
|---|---|---|---|---|
| | | | X-direction | Y-direction |
| M13 | 1 | 1.00 | 0.00 | 79.12 |
| | 2 | 0.95 | 73.23 | 0.00 |
| | 3 | 0.33 | 0.00 | 12.27 |
| | 4 | 0.32 | 0.75 | 0.00 |
| | 5 | 0.26 | 14.35 | 0.00 |
| | | **Sum:** | **88.33** | **91.39** |
| M25 | 1 | 1.07 | 39.15 | 0.00 |
| | 2 | 1.00 | 0.00 | 79.34 |
| | 3 | 0.78 | 35.48 | 0.00 |
| | 4 | 0.33 | 0.00 | 12.21 |
| | 5 | 0.31 | 6.05 | 0.00 |
| | 6 | 0.22 | 8.42 | 0.00 |
| | | **Sum:** | **89.10** | **91.55** |
| M36 | 1 | 1.38 | 10.12 | 0.00 |
| | 2 | 1.00 | 0.00 | 79.40 |
| | 3 | 0.86 | 64.44 | 0.00 |
| | 4 | 0.40 | 1.53 | 0.00 |
| | 5 | 0.33 | 0.00 | 12.16 |
| | 6 | 0.24 | 12.14 | 0.00 |
| | | **Sum:** | **88.23** | **91.56** |

*Table 5 - List of the 48 buildings with stability issues.*

| Model No. | | *R*-factor | Bays span (m) | Number of stories | Location of stability issue |
|---|---|---|---|---|---|
| $\theta = 0.1$ | $\theta = 0.2$ | | | | |
| M49 | M73 | 3.5 | 6 | 5 | First story |
| M50 | M74 | 8.0 | | | |
| M51 | M75 | 3.5 | 10 | | |
| M52 | M76 | 8.0 | | | |
| M53 | M77 | 3.5 | 6 | 10 | |
| M54 | M78 | 8.0 | | | |
| M55 | M79 | 3.5 | 10 | | |
| M56 | M80 | 8.0 | | | |
| M57 | M81 | 3.5 | 6 | 5 | Middle story |
| M58 | M82 | 8.0 | | | |
| M59 | M83 | 3.5 | 10 | | |
| M60 | M84 | 8.0 | | | |
| M61 | M85 | 3.5 | 6 | 10 | |
| M62 | M86 | 8.0 | | | |
| M63 | M87 | 3.5 | 10 | | |
| M64 | M88 | 8.0 | | | |
| M65 | M89 | 3.5 | 6 | 5 | Top story |
| M66 | M90 | 8.0 | | | |
| M67 | M91 | 3.5 | 10 | | |
| M68 | M92 | 8.0 | | | |
| M69 | M93 | 3.5 | 6 | 10 | |
| M70 | M94 | 8.0 | | | |
| M71 | M95 | 3.5 | 10 | | |
| M72 | M96 | 8.0 | | | |

FEMA 440's [4] CSM is a way of estimating the maximum inelastic deformation of a nonlinear structure under earthquake ground motion. It involves converting the force-deformation relationship of the structure and the seismic demand into acceleration-displacement response spectrum (ADRS) format, which plots acceleration versus displacement as depicted in Fig. 7. The method then finds an equivalent linear system that has a larger period and damping than the original nonlinear system. The equivalent period and damping depend on the displacement, the post-yield stiffness, and the hysteretic behavior of the structure. The method uses an iterative process to find the intersection of the capacity curve and the reduced demand curve, which is called the performance point as depicted in Fig. 8. The method also imposes limits on the equivalent damping to account for strength and stiffness degradation. The method uses different parameters and formulas for different types of structures, such as reinforced concrete buildings.

The MPA [9,10] method is a way of estimating the seismic demands for a multistorey building. It involves computing the linear elastic modes and frequencies of the building and performing a nonlinear static analysis for each mode using a force distribution that depends on the mode shape. In this method, the pushover curve in the dominant direction of motion

is converted to an idealized force-deformation ($F_{sn}/L_n$ –$D_n$) relation for the $n^{th}$ mode for an equivalent SDOF system. The SDOF system is idealized as a bilinear curve with a post-yield stiffness that may be negative due to P-Δ effects. The peak deformation of the SDOF system is computed from a nonlinear response history analysis, an inelastic design spectrum, or an elastic design spectrum with empirical equations. The peak roof displacement associated with each mode is obtained by multiplying the peak deformation by the mode shape value at the roof. The peak responses due to gravity and lateral loads are extracted from the pushover database. The dynamic response due to each mode is calculated by subtracting the gravity response from the combined response. The total response is determined by combining the modal responses using the CQC rule.

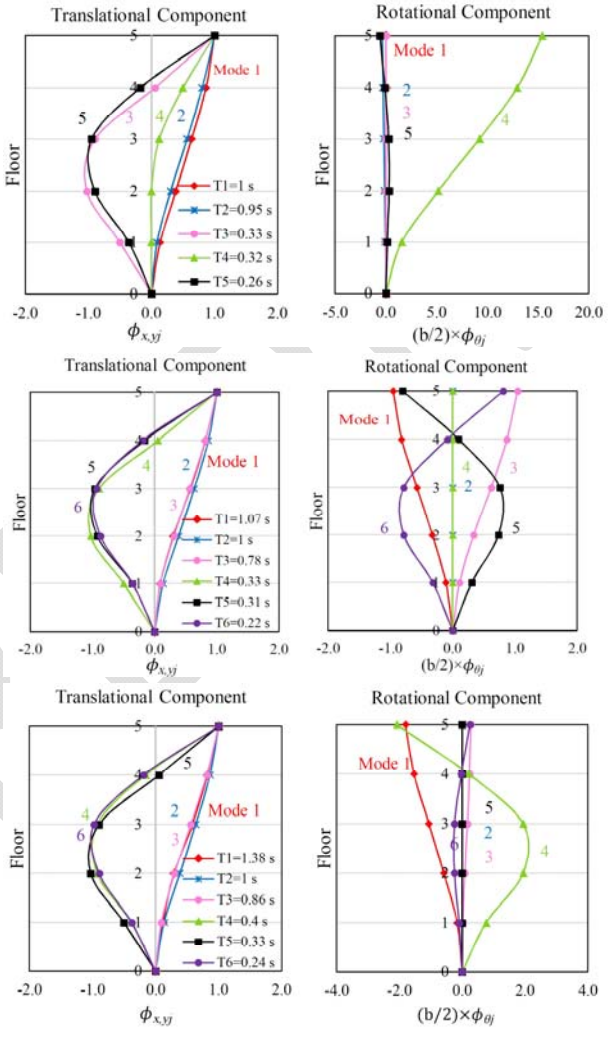


*Fig. 6 - Vibrational modes of three 5-story buildings with plan asymmetries of (a) Type 1 (model M13), (b) Type 2 (model M25), and (c) Type 3 (model M37).*

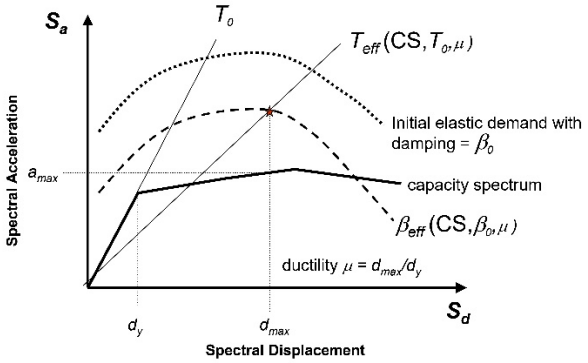


*Fig. 7 - Schematic of ADRS showing effective period and damping parameters of equivalent linear system, along with a capacity curve [4].*

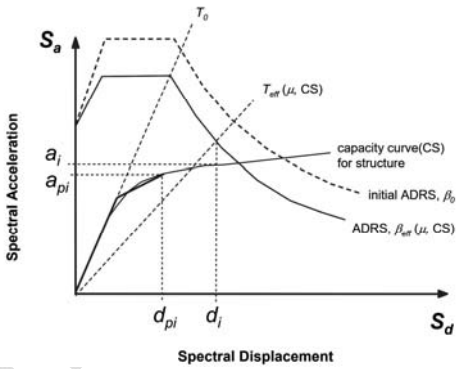


*Fig. 8 - Determination of estimated maximum displacement using direct iteration [4].*

### 4.2. Discussion of Results

The relative errors of inter-story drift ratios and base shears, evaluated using Equation (9), obtained from CSM and MPA approaches for the 12 symmetric buildings with respect to the NTHA evaluations are given in Table 6.

$$e = \frac{R_{Approximation} - R_{NTHA}}{R_{NTHA}} \tag{9}$$

where $e$ represents the relative error, $R_{NTHA}$ denotes the target NTHA response of the system—such as drifts and base shears—averaged across seven earthquake records. $R_{Approximation}$ refers to the corresponding system response estimated using either the CSM or MPA methods. Consequently, negative errors indicate unconservative approximations, while positive errors suggest conservative approximations. Moreover, correlation values and medians of relative errors of the data obtained from analyzing the 96 considered buildings

are reported in Table 7. Since almost all errors are positive, it can be concluded that both methods can be regarded as conservative for symmetric buildings. The results of Table 6 along with the median errors and correlation values given in Table 7 suggest that both CSM and MPA give conservatively correlated approximations of the responses of symmetric buildings. It was also observed that CSM and MPA could overestimate base shears up to 42% and 21% for symmetric buildings, respectively. The overestimation for inter-story drifts could be up to 104% and 96% in worst cases, respectively.

Fig. 9 depicts the base shear relative errors of CSM and MPA procedures with respect to NTHA evaluations corresponding to the 36 asymmetric buildings. The three types of buildings (i.e., Type 1, 2, and 3) are also categorized in this figure. Type 1 buildings were intended to represent asymmetric buildings in which the lateral modes of vibrations are dominant while Type 2 and 3 were intended to represent asymmetric buildings in which lateral-torsional, and torsional modes of vibrations are dominant, respectively. Fig. 9 reveals that although CSM and MPA may yield errors up to 32% and 42% in base shear estimations, respectively, the results lie on the conservative side and are thus safe to use. A similar conclusion can also be drawn from Fig. 10 for inter-story drift responses. Moreover, Table 7 confirms that the base shear responses obtained from CSM and MPA procedures for the 36 asymmetric buildings are highly correlated with those obtained from the NTHAs and thus the results given in Fig. 9 are meaningful. Hence, it may be concluded that both CSM and MPA can be used for conservative seismic evaluation of asymmetric buildings in which lateral modes of vibration are dominant but, regarding the error fluctuations of Figs. 9 and 10 as well as medians of Table 5, it cannot be prescribed which one performs better. Finally, although both methods are conservative for Type 1 buildings, it must be noted that, according to Fig. 9, CSM and MPA might overestimate the base shear up to 31% and 42%, respectively. For inter-story drifts, according to Fig. 10, the overestimations can be up to 90% and 114%, respectively.

For Type 2 buildings, however, Fig. 9 reveals that the base shear responses of CSM and MPA in the X-direction of the buildings were on the unconservative side with relative errors up to -36% and -30% for these methods, respectively. Furthermore, Fig. 10 shows that MPA estimations for inter-story drift ratios were on the conservative side in most cases. According to Table 7, the median of relative errors corresponding to inter-story drifts obtained from MPA was equal to 22% and 39% for X- and Y-directions, respectively. CSM procedure, however, was totally unreliable and unconservative for estimating the inter-story drift-ratios of such buildings because Fig. 10 shows that the responses in one direction of the buildings (i.e., X-direction) were always between -50% and -66% with a median of relative errors, according to Table 7, equal to -59% for that direction. The correlation plot for the inter-story drift ratios of the CSM method in the X-direction is given in Fig. 13 (a), which evidently confirms this conclusion. Hence, it could be concluded that firstly, CSM was unconservative and thus unreliable for seismic demand evaluations of buildings in which lateral-torsional modes of vibrations are dominant, and secondly, due to the incorporation of higher modes effects, MPA gave conservative solutions for the evaluation of displacement demands of such buildings but it was still unreliable for estimating the global response (including both displacement and force demands) of Type 2 buildings.

Regarding Type 3 buildings, Fig. 9 reveals that base shear approximations obtained from CSM and MPA were conservative for most buildings with at most -23% relative error in

unconservative cases. The medians of relative errors in Table 7 also support this conclusion. Regarding inter-story drift ratios, however, Fig. 10 demonstrates that MPA gave conservative approximations while CSM totally underestimated inter-story drift ratios with unconservative errors ranging from -37% to -59%. This conclusion can also be confirmed by the median errors in Table 7 and the correlation plot given in Fig. 13 (a). Thus, it can be concluded that MPA can be regarded as a conservative tool for seismic evaluations of asymmetric buildings in which torsional modes of vibration are dominant while the CSM should be considered an unreliable method. However, it is added that, according to Figs. 9 and 10, MPA can overestimate base shear and inter-story drifts up to 20% and 112%, respectively.

Figs. 11 and 12 illustrate the relative errors of the base shear and inter-story drift ratios of the 48 buildings with different stability coefficients, respectively. The stability coefficients were considered as a code-based indicator of the effects of geometric nonlinearity (i.e., P-Δ effects) on the seismic response of buildings. By investigating Figs. 11 and 12 along with Table 7, which shows high correlations between the results of the approximation techniques and those from NTHA, it can be concluded that the stability issue has an inverse impact on the reliability of CSM and MPA procedures. In other words, in buildings where P-Δ effects are insignificant (i.e., $\theta \leq 1$), both CSM and MPA approximations are relatively reliable (with up to -40% errors on the unconservative side and the medians of the errors ranging from -1.3% to 29%), though it must be emphasized that, in this case, CSM can overestimate base shears and inter-story drifts up to 23% and 26%, while these values for MPA are 35% and 46%, respectively. For buildings where P-Δ effects are significant (i.e., $\theta > 1$), however, both CSM and MPA procedures are unreliable since they yield unconservative approximations with errors up to more than -50% and medians of the errors ranging from -17% to 8%. As an example, the correlation plot for the Y-direction inter-story drift ratios of the CSM approximations is given in Fig. 13(b), where it can be evidently observed that the method yields unconservative solutions for most of the cases.

*Table 6 - Relative errors of CSM and MPA responses vs. NTHA evaluations for the 12 symmetric buildings in Y-dir.*

| Model No. | Average inter-story drifts relative error (%) | | Base shear relative error (%) | |
|---|---|---|---|---|
| | CSM | MPA | CSM | MPA |
| **M1** | 11.45 | 13.23 | 2.98 | 5.12 |
| **M2** | 16.34 | 19.34 | 0.45 | 8.65 |
| **M3** | 95.76 | 103.56 | 12.23 | 18.23 |
| **M4** | 13.94 | 21.76 | 4.53 | 5.97 |
| **M5** | 4.78 | 6.44 | 7.95 | 9.34 |
| **M6** | 66.65 | 89.52 | 17.45 | 43.21 |
| **M7** | 10.56 | 25.19 | 13.29 | 7.45 |
| **M8** | 32.09 | 51.36 | 17.25 | 10.56 |
| **M9** | 46.70 | 35.38 | -3.98 | 7.75 |
| **M10** | 37.28 | 31.34 | 7.90 | 6.43 |
| **M11** | 34.68 | 60.23 | 13.87 | 11.87 |
| **M12** | 18.14 | 13.38 | 13.98 | 20.13 |

*Table 7 - Data correlation and median relative errors of 97 building responses from CSM and MPA vs. NTHA in both directions.*

| Models | Approximation method | Buildings characteristics | Inter-story drifts ratios | | | | Base shears | | | |
|---|---|---|---|---|---|---|---|---|---|---|
| | | | Median of relative error (%) | | Correlation | | Median of relative error (%) | | Correlation | |
| | | | X-direction | Y-direction | X-direction | Y-direction | X-direction | Y-direction | X-direction | Y-direction |
| The 12 symmetric buildings (models M1– M12) | MPA | Symmetric | 2.43 | 28.27 | 0.93 | 0.85 | 5.33 | 9.00 | 0.98 | 0.99 |
| | CSM | | 11.32 | 25.12 | 0.91 | 0.81 | 4.43 | 10.09 | 0.97 | 0.99 |
| The 36 buildings with asymmetric plans (models M13– M48) | MPA | Type 1 | 15.23 | 42.22 | 0.84 | 0.87 | 2.12 | 9.22 | 0.97 | 0.99 |
| | | Type 2 | 22.14 | 39.39 | 0.81 | 0.85 | -5.34 | 9.41 | 0.97 | 0.99 |
| | | Type 3 | 18.08 | 29.35 | 0.93 | 0.84 | 2.98 | 8.30 | 0.97 | 0.99 |
| | CSM | Type 1 | 34.24 | 20.19 | 0.75 | 0.84 | 9.95 | 13.50 | 0.95 | 0.99 |
| | | Type 2 | -59.43 | 0.45 | 0.89 | 0.68 | -15.46 | 16.11 | 0.97 | 0.99 |
| | | Type 3 | -48.12 | 13.43 | 0.90 | 0.81 | 5.45 | 14.48 | 0.97 | 0.99 |
| The 48 buildings with different stability conditions (models M48– M96) | MPA | $\theta = 0.1$ | 3.33 | 29.33 | 0.91 | 0.93 | 5.88 | -1.27 | 0.98 | 0.96 |
| | | $\theta = 0.2$ | 2.67 | 3.67 | 0.91 | 0.97 | 6.66 | -17.19 | 0.98 | 0.92 |
| | CSM | $\theta = 0.1$ | 8.66 | 28.32 | 0.90 | 0.93 | 8.67 | 9.67 | 0.97 | 0.97 |
| | | $\theta = 0.2$ | 8.33 | 6.33 | 0.88 | 0.88 | 8.33 | -14.66 | 0.96 | 0.93 |

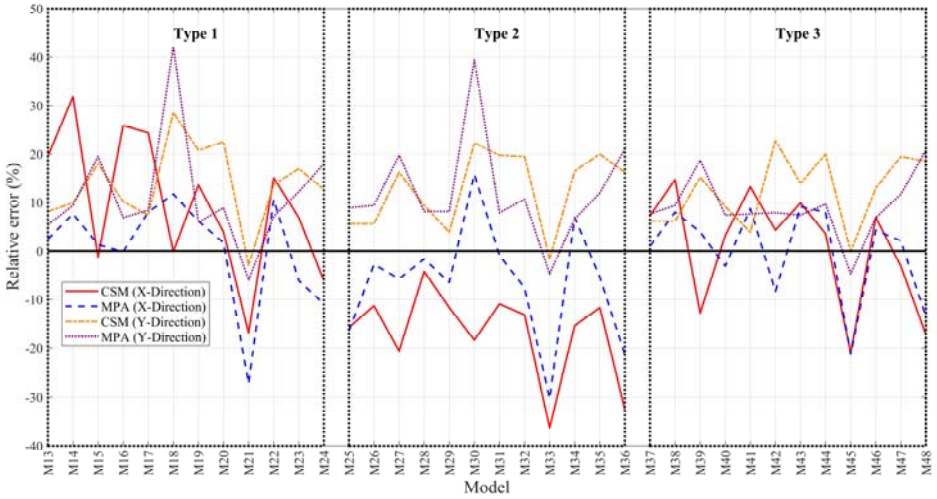


*Fig. 9 - Base shear relative errors of CSM and MPA vs. NTHA for the 36 asymmetric buildings.*

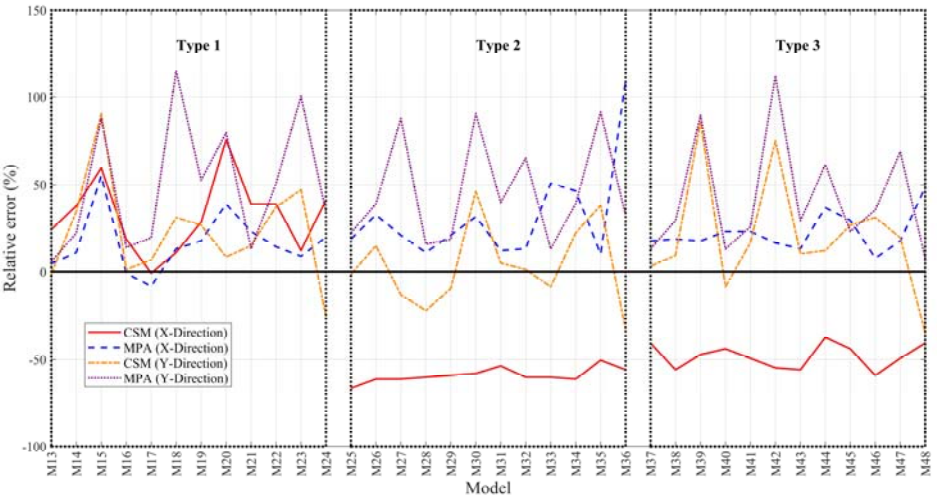


*Fig. 10 - Inter-story drift relative errors of CSM and MPA vs. NTHA for the 36 asymmetric buildings.*

The impact of stability issue location can be explored using Figs. 11 and 12. Significant P-Δ effects ($\theta > 1$) lead to a trend. This trend shows in both figures. As stability issues move to higher stories, errors in estimations grow. These errors lean towards unconservative results for both CSM and MPA methods. When P-Δ effects are minor ($\theta < 1$), the trend persists.

However, there's a distinction. The MPA method shows more unconservative errors than CSM. This is especially true when the stability issue is at the top story.

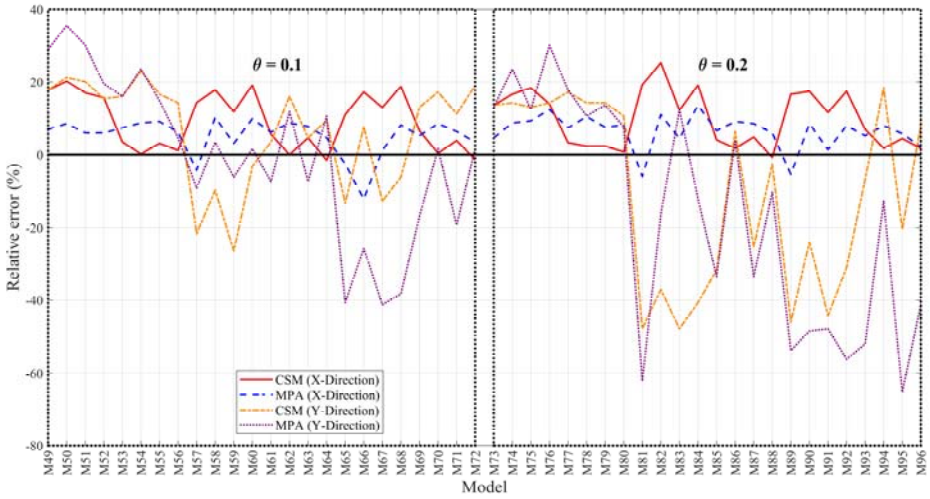


*Fig. 11 - Base shear relative errors of CSM and MPA vs. NTHA for the 48 buildings with different stability conditions.*

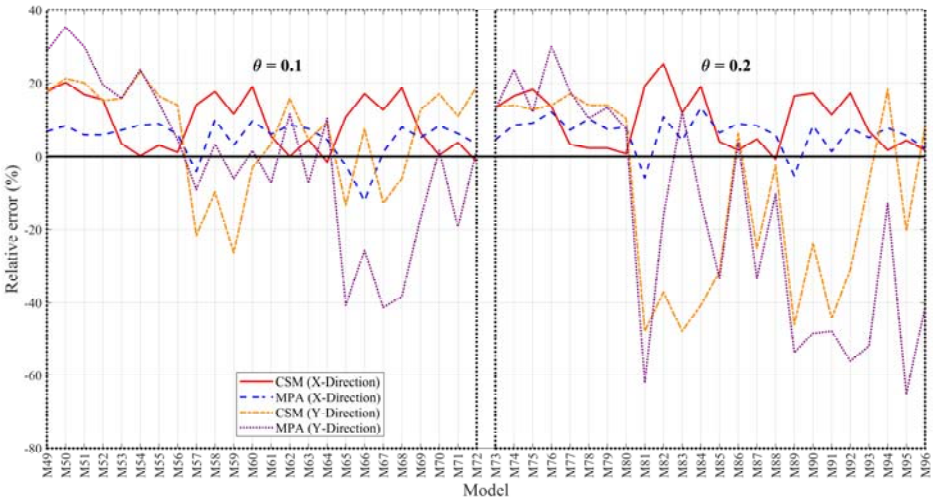


*Fig. 12 - Inter-story drift ratio relative errors of CSM and MPA vs. NTHA for the 48 buildings with different stability conditions.*

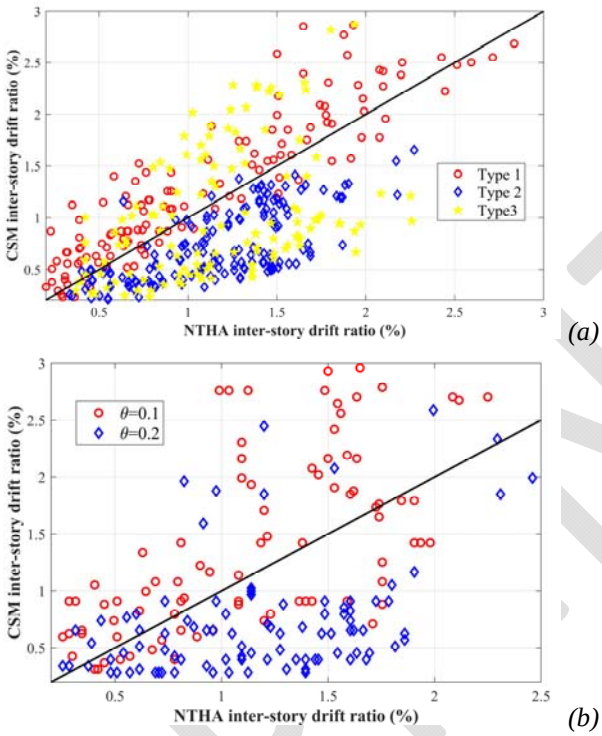


*Fig. 13 - Correlation between CSM approximations and NTHA of inter-story drift ratios for (a) the X-dir responses of the 36 asymmetric buildings, and (b) the Y-dir responses of the 48 buildings with different stability conditions.*

## 5. SUMMARY AND CONCLUSIONS

ASCE/SEI 41-23's [5] coefficient method is a viable codified tool for practitioners to perform the PBSD of buildings. It is true that, compared to linear procedures, the coefficient method can better describe the performance of a structure. However, it is not precise and it does not have the ability to capture the changes in dynamic response as the structure loses stiffness. Also, it cannot handle higher mode effects for multi degree of freedom systems. ASCE/SEI 41-23 [5] restricts the application of the method for two situations: (1) if the effects of higher modes are not negligible (e.g., in irregular buildings), and (2) if the building experiences severe stiffness degradation. In this paper, 1250 SDOF systems were considered to compare their responses from the coefficient method for near- and far-fault sites with the responses obtained from ASCE/SEI 41-23 [5] NDP procedure. It was shown that the method is unreliable for near-fault zones. The errors of base-shear evaluations can be non-conservative by up to 40%. Regarding far-fault zones, it was demonstrated that the method was conservative for systems with small fundamental periods and non-conservative for those with higher fundamental periods (i.e., mid- to high-rise buildings). Hence, it is concluded that further limitations on the applicability of ASCE/SEI 41-23's [5] coefficient method is needed.

Furthermore, for systems with significantly higher mode contributions, the applicability of two approaches, FEMA 440's [4] CSM and MPA [9,10], was investigated. 96 3D buildings were considered, including 12 symmetrical buildings, 36 irregular buildings and 48 buildings with different stability conditions (i.e., stability coefficients of 0.1 or 0.2). The 36 buildings consisted of three types of buildings in which lateral, lateral-torsional, or torsional modes of vibrations were dominant.

Comparing the responses of the 12 symmetric buildings analyzed using the CSM and MPA procedures to those analyzed with NTHAs, it was shown that the median of the errors ranged from 2% to 29%. Both methods were found to be conservative and reliable for the seismic evaluation of symmetric buildings..

The results demonstrated that both CSM and MPA could conservatively be used for approximating the response of irregular buildings in which the lateral modes of vibration were dominant. However, for irregular buildings in which the combination of lateral-torsional modes of vibration was dominant both methods underestimated the responses, resulting in non-conservative errors of up to -66% and -30%, respectively. It was also observed that MPA could yield relatively conservative solutions for the inter-story drift approximations but could not give satisfactory approximations of the base shear of such buildings. The MPA approach could conservatively predict the response of irregular buildings in which torsional modes of vibrations were more dominant but the CSM substantially underestimated the response with non-conservative errors ranging from -37% to -59%.

Finally, regarding the 48 buildings with different stability conditions, it was concluded that if the impact of P-Δ effects on system responses are negligible (i.e., $\theta \leq 1$), both CSM and MPA approximations are relatively conservative, but if the impact of P-Δ effects on system responses is significant (i.e., $\theta > 1$), both CSM and MPA procedures non-conservatively underestimate the building responses. The results also suggest that when the stability issue of the building is shifted to upper stories, response estimations obtained from both methods tend to lean toward the unconservative side.

It could be emphasized that although CSM and MPA can be conservatively adopted in some cases as discussed in preceding paragraphs, it was shown that the overestimation errors could be very large such that it undermines the applications of these methods from the economical viewpoint. Thus, it is recommended that at least the final design be cross-checked using NTHAs.

**List of symbols**

| | |
|---|---|
| $a$ | Site class factor |
| $a_0$ | Constant stiffness coefficient |
| $a_1$ | Constant mass coefficient |
| $C_0$ | Spectral displacement modification factor |
| $C_1$ | Maximum displacement ratio coefficient |
| $C_2$ | Hysteresis modification factor |

| | |
|---|---|
| $C_m$ | Effective mass factor |
| $F_u$ | Ultimate stress |
| $F_y$ | Yield stress |
| $g$ | Gravitational acceleration |
| $h_{sx}$ | Story height below level *x* |
| $\mathbf{K}$ | Initial stiffness matrix |
| $K_e$ | Effective lateral stiffness |
| $K_i$ | Elastic lateral stiffness |
| $\mathbf{K}_t$ | Tangential stiffness matrix |
| $\mathbf{M}$ | Mass matrix |
| $m_i$ | Mass at the $i^{\text{th}}$ story of the building |
| $P_x$ | Vertical design load at and above level *x* |
| $R_{jb}$ | Joyner-Boore distance |
| $R_{rup}$ | Closest distance to the fault rupture |
| $S_a$ | Spectral response acceleration |
| $T_e$ | Effective fundamental period |
| $T_i$ | Elastic fundamental period |
| $V_s$ | Average shear wave velocity |
| $V_x$ | Seismic design shear |
| $W$ | Effective seismic weight |
| $\beta$ | Damping ratio |
| $\delta_t$ | Target displacement |
| $\Delta_{xe}$ | Elastic story drift below level *x* |
| $\theta$ | Stability coefficient |
| $\mu$ | Ductility |
| $\mu_{\text{strength}}$ | Elastic strength demand to yield strength ratio |
| $\phi_{1,r}$ | Ordinate of the first mode shape at the roof |
| $\phi_{i,n}$ | Ordinate of mode shape *i* at level *n* of the building |



## References

[1] V. Mokarram, A novel PSO-based multi-objective optimization methodology toward NTH analysis-based design of steel structures, PhD Dissertation, Shiraz University, 2018.

[2] V. Mokarram, M.R. Banan, An improved multi-objective optimization approach for performance-based design of structures using nonlinear time-history analyses, Appl Soft Comput 73 (2018) 647–665. https://doi.org/10.1016/J.ASOC.2018.08.048.

[3] FEMA 356, Prestandard and commentary for the seismic rehabilitation of buildings, Washington, D.C., 2000.

[4] FEMA 440, Improvement of nonlinear static seismic analysis procedures, Washington, D.C., 2005.

[5] ASCE/SEI 41-23, ASCE standard ASCE/SEI 41-23 Seismic evaluation and retrofit of existing buildings, American Society of Civil Engineers, Reston, Virginia, 2023.

[6] FEMA 273, NEHRP guidelines for the seismic rehabilitation of buildings, Washington, D.C., 1997.

[7] P. Fajfar, A nonlinear analysis method for performance-based seismic design, Earthquake Spectra 16 (2000) 573–592. https://doi.org/10.1193/1.1586128.

[8] P. Fajfar, M. Fischinger, N2-A method for non-linear seismic analysis of regular buildings, in: Proceedings of the Ninth World Conference in Earthquake Engineering, 1988: pp. 111–116.

[9] A.K. Chopra, R.K. Goel, A modal pushover analysis procedure to estimate seismic demands for unsymmetric-plan buildings, Earthq Eng Struct Dyn 33 (2004) 903–927. https://doi.org/10.1002/EQE.380.

[10] A.K. Chopra, R.K. Goel, A modal pushover analysis procedure for estimating seismic demands for buildings, Earthq Eng Struct Dyn 31 (2002) 561–582. https://doi.org/10.1002/EQE.144.

[11] T.S. Jan, M.W. Liu, C. Kao Ying Chieh, An upper-bound pushover analysis procedure for estimating the seismic demands of high-rise buildings, Eng Struct 26 (2004) 117–128. https://doi.org/10.1016/J.ENGSTRUCT.2003.09.003.

[12] E. Kalkan, S.K. Kunnath, Adaptive modal combination procedure for nonlinear static analysis of building structures, Journal of Structural Engineering 132 (2006) 1721–1731. https://doi.org/10.1061/(ASCE)0733-9445(2006)132:11(1721).

[13] C. Casarotti, R. Pinho, An adaptive capacity spectrum method for assessment of bridges subjected to earthquake action, Bulletin of Earthquake Engineering 5 (2007) 377–390. https://doi.org/10.1007/S10518-007-9031-8/METRICS.

[14] M. Poursha, F. Khoshnoudian, A.S. Moghadam, A consecutive modal pushover procedure for estimating the seismic demands of tall buildings, Eng Struct 31 (2009) 591–599. https://doi.org/10.1016/J.ENGSTRUCT.2008.10.009.

[15] H. Sucuoğlu, M.S. Günay, Generalized force vectors for multi-mode pushover analysis, Earthq Eng Struct Dyn 40 (2011) 55–74. https://doi.org/10.1002/EQE.1020.

[16] M. Zarrin, A. Daei, T. Heydary, A simplified normalized multi-mode nonlinear static procedure (NMP) for seismic performance evaluation of building structures, Bulletin of Earthquake Engineering 19 (2021) 5711–5741. https://doi.org/10.1007/S10518-021-01185-Y/METRICS.

[17] E. Kalkan, S.K. Kunnath, Assessment of current nonlinear static procedures for seismic evaluation of buildings, Eng Struct 29 (2007) 305–316. https://doi.org/10.1016/J.ENGSTRUCT.2006.04.012.

[18] R. Bento, C. Bhatt, R. Pinho, Using nonlinear static procedures for seismic assessment of the 3D irregular SPEAR building, Earthquakes and Structures 1 (2010) 177–195.

[19] R. Pinho, M. Marques, R. Monteiro, C. Casarotti, R. Delgado, Evaluation of nonlinear static procedures in the assessment of building frames, Earthquake Spectra 29 (2013) 1459–1476. https://doi.org/10.1193/100910EQS169M.

[20] M. Fragiadakis, D. Vamvatsikos, M. Aschheim, Application of nonlinear static procedures for the seismic assessment of regular RC moment frame buildings, Earthquake Spectra 30 (2014) 767–794. https://doi.org/10.1193/111511EQS281M.

[21] R. Allahvirdizadeh, Y. Gholipour, Reliability evaluation of predicted structural performances using nonlinear static analysis, Bulletin of Earthquake Engineering 15 (2017) 2129–2148. https://doi.org/10.1007/s10518-016-0062-x.

[22] R. Gonzalez-Drigo, J. Avila-Haro, L.G. Pujades, A.H. Barbat, Non-linear static procedures applied to high-rise residential URM buildings, Bulletin of Earthquake Engineering 15 (2017) 149–174. https://doi.org/10.1007/s10518-016-9951-2.

[23] S. Marino, S. Cattari, S. Lagomarsino, Are the nonlinear static procedures feasible for the seismic assessment of irregular existing masonry buildings?, Eng Struct 200 (2019) 109700. https://doi.org/10.1016/J.ENGSTRUCT.2019.109700.

[24] S. Ruggieri, G. Uva, Accounting for the spatial variability of seismic motion in the pushover analysis of regular and irregular RC buildings in the new Italian building code, Buildings 2020, Vol. 10, Page 177 10 (2020) 177. https://doi.org/10.3390/BUILDINGS10100177.

[25] A. Daei, M. Poursha, On the accuracy of enhanced pushover procedures for seismic performance evaluation of code-conforming RC moment-resisting frame buildings subjected to pulse-like and non-pulse-like excitations, Structures 32 (2021) 929–945. https://doi.org/10.1016/J.ISTRUC.2021.03.035.

[26] M. Ferraioli, Dynamic increase factor for nonlinear static analysis of RC frame buildings against progressive collapse, International Journal of Civil Engineering 17 (2019) 281–303. https://doi.org/10.1007/s40999-017-0253-0.

[27] K. Ke, F. Wang, M.C.H. Yam, L. Deng, Y. He, A multi-stage-based nonlinear static procedure for estimating seismic demands of steel MRFs equipped with steel slit walls, Eng Struct 183 (2019) 1091–1108. https://doi.org/10.1016/J.ENGSTRUCT.2019.01.029.

[28] R. Couto, M. V. Requena-García-Cruz, R. Bento, A. Morales-Esteban, Seismic capacity and vulnerability assessment considering ageing effects: case study—three local Portuguese RC buildings, Bulletin of Earthquake Engineering 19 (2021) 6591–6614. https://doi.org/10.1007/s10518-020-00955-4.

[29] J. Wang, X. Wang, A. Ye, Z. Guan, Deformation-based pushover analysis method for transverse seismic assessment of inverted Y-shaped pylons in kilometer-span cable-stayed bridges: Formulation and application to a case study, Soil Dynamics and Earthquake Engineering 169 (2023) 107874. https://doi.org/10.1016/J.SOILDYN.2023.107874.

[30] T. Rossetto, C. De la Barra, C. Petrone, J.C. De la Llera, J. Vásquez, M. Baiguera, Comparative assessment of nonlinear static and dynamic methods for analysing building response under sequential earthquake and tsunami, Earthq Eng Struct Dyn 48 (2019) 867–887. https://doi.org/10.1002/EQE.3167.

[31] M. Bhandari, S.D. Bharti, M.K. Shrimali, T.K. Datta, Seismic fragility analysis of base-isolated building frames excited by near- and far-field earthquakes, Journal of Performance of Constructed Facilities 33 (2019) 04019029. https://doi.org/10.1061/(ASCE)CF.1943-5509.0001298.

[32] V. Mokarram, M.R. Banan, M.R. Banan, Reliability of the maximum displacement ratio in nonlinear static procedure for near-fault sites, in: International Conference on Civil Engineering, Architecture and Urban Management in Iran, Tehran, Iran, 2018: pp. 1–6. https://civilica.com/doc/846835/ (accessed August 25, 2023).

[33] H. Bilgin, M. Hysenlliu, Comparison of near and far-fault ground motion effects on low and mid-rise masonry buildings, Journal of Building Engineering 30 (2020) 101248. https://doi.org/10.1016/J.JOBE.2020.101248.

[34] A. Mortezaei, H.R. Ronagh, A. Kheyroddin, G.G. Amiri, Effectiveness of modified pushover analysis procedure for the estimation of seismic demands of buildings subjected to near-fault earthquakes having forward directivity, The Structural Design of Tall and Special Buildings 20 (2011) 679–699. https://doi.org/10.1002/TAL.553.

[35] A.V. Bergami, G. Fiorentino, D. Lavorato, B. Briseghella, C. Nuti, Application of the incremental modal pushover analysis to bridges subjected to near-fault ground motions, Applied Sciences 2020, Vol. 10, Page 6738 10 (2020) 6738. https://doi.org/10.3390/APP10196738.

[36] A. Asıkoğlu, G. Vasconcelos, P.B. Lourenço, Overview on the nonlinear static procedures and performance-based approach on modern unreinforced masonry buildings with structural irregularity, Buildings 2021, Vol. 11, Page 147 11 (2021) 147. https://doi.org/10.3390/BUILDINGS11040147.

[37] P.K. Das, S.C. Dutta, T.K. Datta, Seismic behavior of plan and vertically irregular structures: state of art and future challenges, Nat Hazards Rev 22 (2020) 04020062. https://doi.org/10.1061/(ASCE)NH.1527-6996.0000440.

[38] F.A. Najam, Nonlinear static analysis procedures for seismic performance evaluation of existing buildings – evolution and issues, Sustainable Civil Infrastructures (2018) 180–198. https://doi.org/10.1007/978-3-319-61914-9_15/FIGURES/9.

[39] W.M. Hassan, J.C. Reyes, Assessment of modal pushover analysis for mid-rise concrete buildings with and without viscous dampers, Journal of Building Engineering 29 (2020) 101103. https://doi.org/10.1016/J.JOBE.2019.101103.

[40] D.G. Lignos, H. Krawinkler, Deterioration modeling of steel components in support of collapse prediction of steel moment frames under earthquake loading, Journal of Structural Engineering 137 (2011) 1291–1302. https://doi.org/10.1061/(ASCE)ST.1943-541X.0000376.

[41] F. Zareian, R.A. Medina, A practical method for proper modeling of structural damping in inelastic plane structural systems, Comput Struct 88 (2010) 45–53. https://doi.org/10.1016/j.compstruc.2009.08.001.

[42] S. Mazzoni, F. McKenna, M.H. Scott, G.L. Fenves, The open system for earthquake engineering simulation (OpenSees) user command-language manual, (2006).

[43] D.G. Lignos, H. Krawinkler, A steel database for component deterioration of tubular hollow square steel columns under varying axial load for collapse assessment of steel structures under earthquakes, in: 7th International Conference on Urban Earthquake Engineering (7CUEE) & 5th International Conference on Earthquake Engineering (5ICEE) Conf. on Urban Earthquake Engineering (7CUEE), Tokyo: Center for Urban Earthquake Engineering, Tokyo Institute of Technology., 2010.

[44] D.G. Lignos, H. Krawinkler, Sidesway collapse of deteriorating structural systems under seismic excitations, Report No. 177, The John A. Blume Earthquake Engineering Center, Stanford University, Stanford, CA, 2012.

[45] J.F. Hall, Problems encountered from the use (or misuse) of Rayleigh damping, Earthq Eng Struct Dyn 35 (2006) 525–545. https://doi.org/10.1002/eqe.541.

[46] L. Petrini, C. Maggi, M.J.N. Priestley, G.M. Calvi, Experimental verification of viscous damping modeling for inelastic time history analyzes, Journal of Earthquake Engineering 12 (2008) 125–145. https://doi.org/10.1080/13632460801925822.

[47] V. Mokarram, M.R. Banan, Modeling considerations for performance based seismic design of steel moment resisting frames, in: International Conference on Civil Engineering, Architecture and Urban Management in Iran, Tehran, Iran, 2018: pp. 1–14. https://civilica.com/doc/846834/.

[48] ASCE/SEI 7-22, ASCE standard ASCE/SEI 7-22 Minimum design loads for buildings and other structures, American Society of Civil Engineers, Reston, Virginia, 2022.

[49] ANSI/AISC 360-22, ANSI/AISC 360-22 An American national standard specification for structural steel buildings, American Institute of Steel Construction, Chicago, Illinois, 2022.

[50] A. Neuenhofer, F.C. Filippou, Evaluation of nonlinear frame finite-element models, Journal of Structural Engineering 123 (1997) 958–966. https://doi.org/10.1061/(ASCE)0733-9445(1997)123:7(958).

[51] B.N. Alemdar, D.W. White, Displacement, flexibility, and mixed beam–column finite element formulations for distributed plasticity analysis, Journal of Structural Engineering 131 (2005) 1811–1819. https://doi.org/10.1061/(ASCE)0733-9445(2005)131:12(1811).

[52] S.M. Kostic, F.C. Filippou, Section discretization of fiber beam-column elements for cyclic inelastic response, Journal of Structural Engineering 138 (2012) 592–601. https://doi.org/10.1061/(ASCE)ST.1943-541X.0000501.

**Appendix 1**

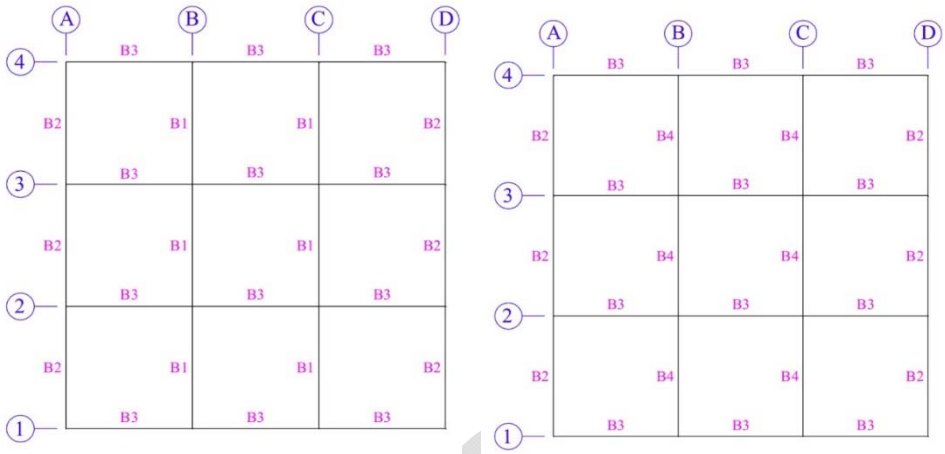


*(a)* *(b)*

*Fig. A1 - Grouping of the beams of the basic 5-story buildings: (a) 1st and 2nd stories, and (b) 3rd, 4th, and 5th stories.*

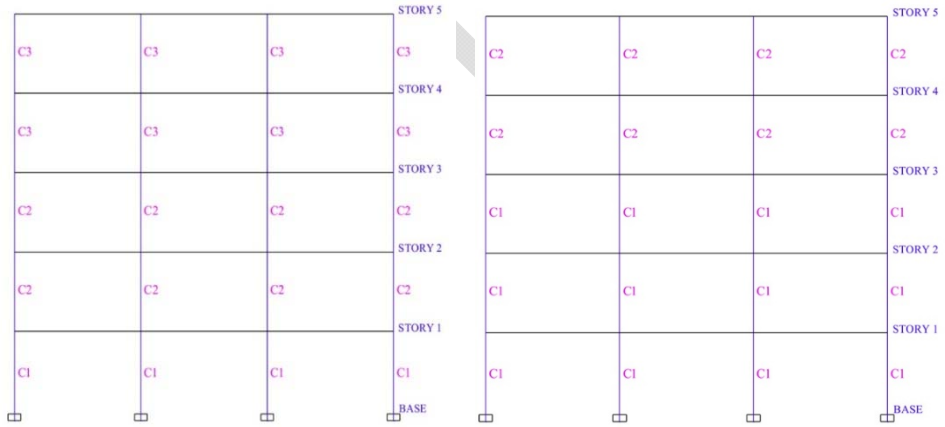


*(a)* *(b)*

*Fig. A2 - Grouping of the columns of the basic 5-story buildings: (a) axis 1, and 4, and (b) axis 2, and 3.*

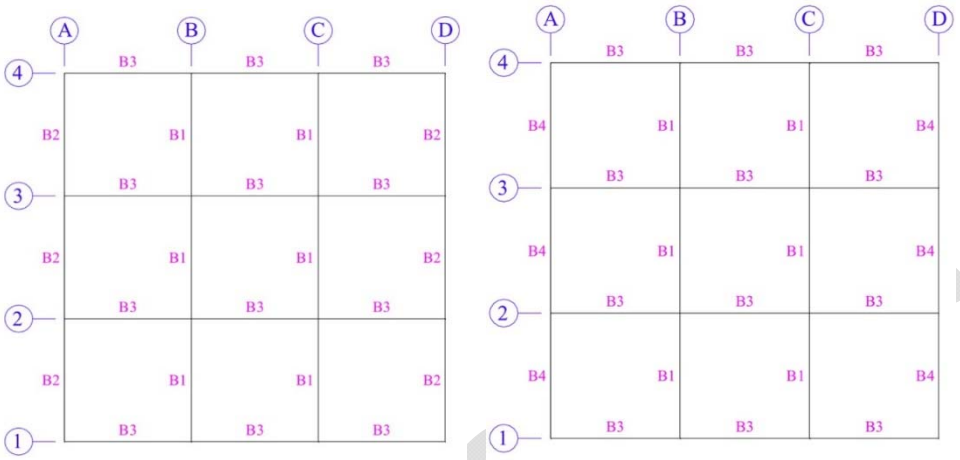


*(a)* *(b)*

*Fig. A3 - Grouping of the beams of the basic 10-story buildings: (a) 1st, 2nd, and 3rd stories, and (b) 4th, and 5th stories.*

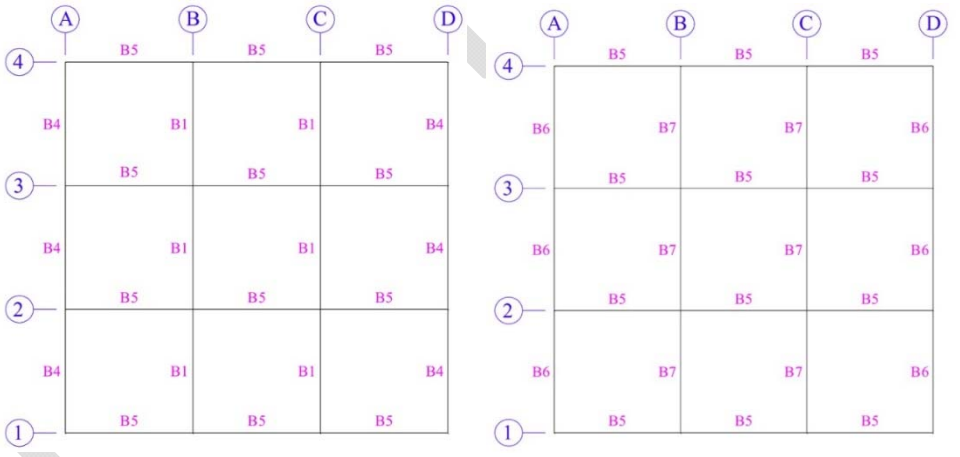


*(a)* *(b)*

*Fig. A4 - Grouping of the beams of the basic 10-story buildings: (a) 6th, and 7th stories, and (b) 8th, 9th, and 10th stories.*

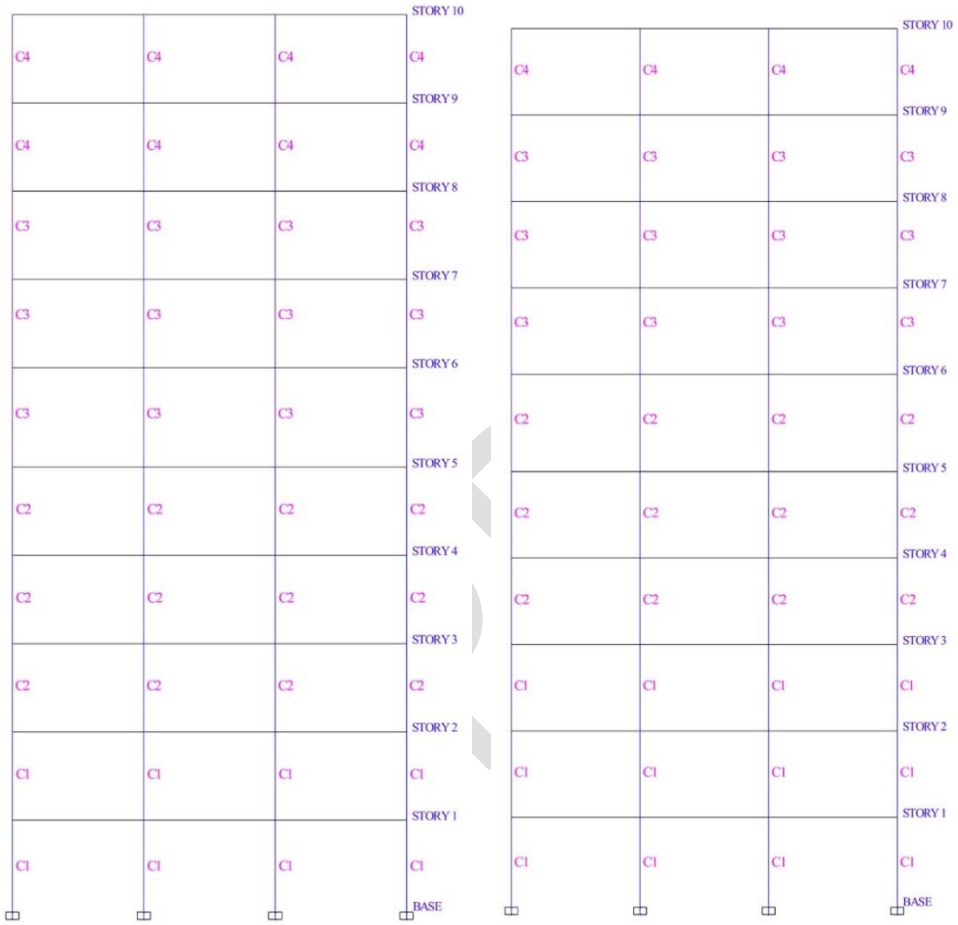


*(a)* *(b)*

*Fig. A5 - Grouping of the columns of the basic 10-story buildings: (a) axis 1, and 4, and (b) axis 2, and 3.*

*Table A1 - List of sections of the 12 basic buildings.*

| Model No. | C1 | C2 | C3 | C4 | B1 | B2 | B3 | B4 | B5 | B6 | B7 |
|---|---|---|---|---|---|---|---|---|---|---|---|
| M1 | 70×55×2 | 55×45×2 | 45×35×2 | N/A | 45×25×2 | 40×20×1 | 40×20×1 | 45×25×1.5 | N/A | N/A | N/A |
| M2 | 55×45×2 | 50×40×2 | 45×35×2 | N/A | 50×30×2 | 40×20×1 | 40×20×1 | 40×20×1 | N/A | N/A | N/A |
| M3 | 50×35×2 | 45×35×2 | 40×30×2 | N/A | 35×20×1 | 30×15×1 | 30×15×1 | 35×20×1 | N/A | N/A | N/A |
| M4 | 85×60×4 | 75×50×4 | 65×40×4 | N/A | 75×40×2 | 60×30×2 | 50×30×2 | 70×30×2 | N/A | N/A | N/A |
| M5 | 70×50×4 | 60×45×4 | 55×35×3 | N/A | 60×35×2 | 60×35×2 | 30×30×2 | 60×35×2 | N/A | N/A | N/A |
| M6 | 60×45×2 | 60×45×2 | 60×45×2 | N/A | 55×30×2 | 45×25×2 | 45×25×2 | 55×30×2 | N/A | N/A | N/A |
| M7 | 60×45×4 | 50×40×4 | 45×35×3 | 40×30×2 | 55×30×2 | 50×20×2 | 50×20×2 | 45×25×2 | 40×20×2 | 45×25×1 | 40×20×2 |
| M8 | 50×40×3 | 450×35×3 | 45×35×2 | 40×30×2 | 45×25×2 | 45×20×1 | 45×20×1 | 40×20×1 | 40×20×1 | 40×20×1 | 40×20×1 |
| M9 | 45×35×2 | 40×30×2 | 30×20×2 | 30×20×2 | 40×20×1 | 30×15×1 | 30×15×1 | 30×15×1 | 30×15×1 | 30×15×1 | 40×20×1 |
| M10 | 85×65×6 | 80×60×6 | 65×50×5 | 50×40×4 | 70×35×4 | 65×35×2 | 70×35×2 | 60×35×2 | 60×35×2 | 55×30×2 | 70×30×2 |
| M11 | 70×55×5 | 65×55×5 | 60×50×5 | 50×40×4 | 70×35×2 | 60×35×2 | 65×30×2 | 50×30×2 | 50×20×2 | 50×30×2 | 50×30×2 |
| M12 | 65×45×4 | 60×40×4 | 55×35×4 | 45×35×4 | 50×30×2 | 40×20×2 | 50×30×1 | 40×20×2 | 45×25×1 | 50×30×2 | 40×20×2 |

**Note:** All sections are I-shaped and are designated in the format: height × width × thickness (in centimeters). “N/A” stands for Not Applicable.

*Table A2 - Sections of columns of the story with stability issue in each building.*

| Model No. | Sections of columns | Model No. | Sections of columns | Model No. | Sections of columns | Model No. | Sections of columns |
|---|---|---|---|---|---|---|---|
| M49 | 70×27×2 | M61 | 50×26×4 | M73 | 70×21×2 | M85 | 50×20×4 |
| M50 | 55×27×2 | M62 | 45×31×3 | M74 | 55×21×2 | M86 | 45×24×3 |
| M51 | 85×30×4 | M63 | 80×35×6 | M75 | 85×23×4 | M87 | 80×28×6 |
| M52 | 70×40×4 | M64 | 65×42×5 | M76 | 70×24×4 | M88 | 65×29×5 |
| M53 | 60×27×4 | M65 | 45×18×2 | M77 | 60×21×4 | M89 | 45×14×2 |
| M54 | 50×30×3 | M66 | 45×18×2 | M78 | 50×24×3 | M90 | 45×14×2 |
| M55 | 85×33×6 | M67 | 65×20×4 | M79 | 85×26×6 | M91 | 65×15×4 |
| M56 | 70×37×5 | M68 | 55×22×3 | M80 | 70×29×5 | M92 | 55×18×3 |
| M57 | 55×26×2 | M69 | 40×19×2 | M81 | 55×20×2 | M93 | 40×15×2 |
| M58 | 50×26×2 | M70 | 40×18×2 | M82 | 50×20×2 | M94 | 40×15×2 |
| M59 | 75×28×4 | M71 | 50×21×4 | M83 | 75×22×4 | M95 | 50×21×2 |
| M60 | 60×30×4 | M72 | 50×22×4 | M84 | 60×22×4 | M96 | 50×21×2 |

**Note:** All columns in the story addressing the stability issue in each building possess identical cross-sectional dimensions, as specified in this table. All sections are I-shaped and are designated in the format: height × width × thickness (in centimeters).